REPORT DOCUMENTATION PAGE

1. REPORT DATE *(DD-MM-YYYY)*	2. REPORT TYPE	3. DATES COVERED *(From - To)*
16-06-2008	Technical Paper	

4. TITLE AND SUBTITLE	5a. CONTRACT NUMBER
Application of the Born-Mayer Potential with a Hard-Sphere Scattering Kernel to Rarefied Hyperthermal Gas Flow Modeling (Preprint)	5b. GRANT NUMBER
	5c. PROGRAM ELEMENT NUMBER

6. AUTHOR(S)	
William Dimpfl (The Aerospace Corporation); Sergey F. Gimelshein (USC); Ingrid Wysong (AFRL/RZSA); Matthew Braunstein & Lawrence Bernstein (Spectral Sciences, Inc.)	5d. PROJECT NUMBER
	5e. TASK NUMBER
	23080532
	5f. WORK UNIT NUMBER

7. PERFORMING ORGANIZATION NAME(S) AND ADDRESS(ES)	8. PERFORMING ORGANIZATION REPORT NUMBER
Air Force Research Laboratory (AFMC) AFRL/RZSA 10 E. Saturn Blvd. Edwards AFB CA 93524-7680	AFRL-RZ-ED-TP-2008-235

9. SPONSORING / MONITORING AGENCY NAME(S) AND ADDRESS(ES)	10. SPONSOR/MONITOR'S ACRONYM(S)
Air Force Research Laboratory (AFMC) AFRL/RZS 5 Pollux Drive Edwards AFB CA 93524-7048	11. SPONSOR/MONITOR'S NUMBER(S) AFRL-RZ-ED-TP-2008-235

12. DISTRIBUTION / AVAILABILITY STATEMENT

Approved for public release; distribution unlimited (PA #08257A).

13. SUPPLEMENTARY NOTES
For presentation at the 26th International Symposium on Rarefied Gas Dynamics, Kyoto, Japan, 21-25 July 2008.

14. ABSTRACT
Mid ultraviolet Cameron band emission from carbon monoxide is seen in plumes of Space Shuttle Orbiter engine burns in low earth orbit. The observed emission has been attributed to chemiluminescence from two and three step chemistry of a minor amount of methane in the plume with atmospheric atomic oxygen. DSMC modeling has played an important role in determining the mechanism, but standard DSMC methods show significant discrepancies in the size and shape of the radiance. The differences have been traced to a need to extend the validity of scattering treatment to hyperthermal ($E_{rel} > 1$ eV) collision energies. Variable Hard Sphere (VHS) and Variable Soft Sphere (VSS) scattering treatments have been based on inverse-power-law repulsive inter-particle potential energy functions. The legacy of such functionality comes from the ability of the Lenard-Jones formalism to produce a realistic potential well and the convenience in mathematical treatments. It is known, however, that such potentials predict interactions that are too stiff at hyperthermal energies when fit to thermal data. Interaction potentials which have been characterized at hyperthermal energies indicate that a Born-Mayer exponential formalism is generally valid to interaction energies up to about 50 eV. Born-Mayer potential formalism has been introduced into DSMC treatment to extend its validity into the hyperthermal regime to define Extended Variable Hard Sphere (EVHS) and Extended Variable Soft Sphere (EVSS) treatments. The addition can be introduced without computational penalty. Comparisons between VHS and EVHS modeling at thermal energies and EVHS with hyperthermal plume radiance data demonstrate the validity of the modification.

15. SUBJECT TERMS

16. SECURITY CLASSIFICATION OF:			17. LIMITATION OF ABSTRACT	18. NUMBER OF PAGES	19a. NAME OF RESPONSIBLE PERSON Dr. Ingrid Wysong
a. REPORT	b. ABSTRACT	c. THIS PAGE			19b. TELEPHONE NUMBER *(include area code)*
Unclassified	**Unclassified**	**Unclassified**	SAR	11	N/A

APPLICATION OF THE BORN-MAYER POTENTIAL WITH A HARD-SPHERE SCATTERING KERNEL TO RAREFIED HYPERTHERMAL GAS FLOW MODELING [*]

William Dimpfl
The Aerospace Corporation, El Segundo, CA 90245

Sergey F. Gimelshein
University of Southern California, Los Angeles, CA 90089

Ingrid J. Wysong
Air force Research Laboratory, Edwards AFB, CA 93524

Matthew Braunstein and Lawrence Bernstein
Spectral Sciences, Inc., Burlington, MA 01803

ABSTRACT

Mid ultraviolet Cameron band emission from carbon monoxide is seen in plumes of Space Shuttle Orbiter engine burns in low earth orbit. The observed emission has been attributed to chemiluminescence from two and three step chemistry of a minor amount of methane in the plume with atmospheric atomic oxygen. DSMC modeling has played an important role in determining the mechanism, but standard DSMC methods show significant discrepancies in the size and shape of the radiance. The differences have been traced to a need to extend the validity of scattering treatment to hyperthermal ($E_{rel} > 1$ eV) collision energies. Variable Hard Sphere (VHS) and Variable Soft Sphere (VSS) scattering treatments have been based on inverse-power-law repulsive inter-particle potential energy functions. The legacy of such functionality comes from the ability of the Lenard-Jones formalism to produce a realistic potential well and the convenience in mathematical treatments. It is known, however, that such potentials predict interactions that are too stiff at hyperthermal energies when fit to thermal data. Interaction potentials which have been characterized at hyperthermal energies indicate that a Born-Mayer exponential formalism is generally valid to interaction energies up to about 50 eV. Born-Mayer potential formalism has been introduced into DSMC treatment to extend its validity into the hyperthermal regime to define Extended Variable Hard Sphere (EVHS) and Extended Variable Soft Sphere (EVSS) treatments. The addition can be introduced without computational penalty. Comparisons between VHS and EVHS modeling at thermal energies and EVHS with hyperthermal plume radiance data demonstrate the validity of the modification.

1. INTRODUCTION AND BACKGROUND

Atomic and molecular interactions at thermal energies are effectively simulated by the Lenard-Jones 6-12 potential:

$$V(r) = 4\varepsilon\,[(r_o/r)^{12} - (r_o/r)^6], \qquad (1)$$

where $V(r)$ is potential energy, ε is the well depth, r_o is the distance where the potential crosses the zero energy axis and r is the inter-nuclear separation. This inverse-power-law potential includes long range forces, which accurately simulate the potential from the attractive r^{-6} London dispersion forces. The shorter range electronic repulsion is treated approximately by the r^{-12} term to yield a potential well that is in reasonable agreement in depth shape and distance of the well bottom with those determined by inversion of data from molecular beam scattering experiments. While the inverse-power functionality for the repulsion does not have a theoretical basis aside from producing monatonic repulsion it produces a repulsive wall that that is generally reasonably accurate up to collision energies of about 0.1 to 1 eV, covering energies relevant to the upper limit to thermal temperatures (~4000K).

Such analytical potentials extend to unlimited distances making their direct use in treating the dynamic interaction of large numbers of interacting particles computationally intractable. This well-known difficulty is managed by treating the particles as Variable Hard Spheres (VHS), discrete hard spheres that vary in size depending on the collision

energy,[1] the scattering being isotropic in a reference frame centered at the collision center of mass. The parameters used in describing hard sphere collisions are shown in Figure 1.
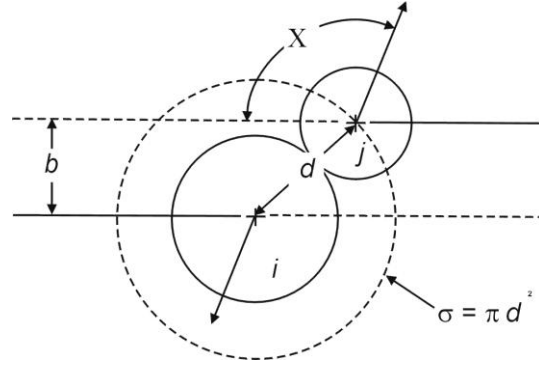

Figure 1. Hard sphere collision between particles i and j, shown in the center of mass frame. The collision cross section, σ, simply equals πd^2, where d is the sum of the radii of the colliding particles. X is the center of mass frame scattering angle which is equal to $2 \cos^{-1}(b/d)$, where b is the center of mass impact parameter.

VHS model discrete particle sizes are defined through theoretical derivation of viscosity from the analytical potential. An important parameter for determining VHS particle sizes in a collision is the viscosity coefficient, ω, which is linked to the repulsive exponent, n, of the inverse power law potential through the relation $\omega = (n + 2)/2n$. The other parameters which characterize VHS particle sizes are a reference diameter, d_{ref}, associated with a reference temperature, T_{ref}. Reference temperatures are also identified with reference relative collision energies through the relation $E_{ref} = 3kT_{ref}/2$ and reference relative collision velocities through their kinetic energy relationship. DSMC including VHS is effective at reproducing temperature dependence of viscosity and other macroscopic observables, such as plume radiance. Such measurable observables have been found to be remarkably insensitive to the somewhat unrealistic isotropic scattering distribution.

Discrepancies are found, however, in the ability of pure isotropic scattering to simultaneously reproduce viscosity and diffusion behavior in DSMC treatment. The Variable Soft Sphere[2] (VSS) model introduces a bias to the isotropic scattering but maintains a discrete cross section, allowing viscosity and diffusion behavior to be accurately treated simultaneously by DSMC.

In applying DSMC techniques to simulate high altitude plume radiance, resulting from interaction of the plume with the residual atmosphere, the size of the observed radiant field is larger than that predicted for spacecraft moving at orbital velocities.[3] These differences were first noticed in analyzing Cameron band radiance in plumes from the Midcourse Space Experiment (MSX) Shuttle Plume Observation experiment, described in reference 3. The Cameron band system of $CO(a\,^3\Pi_r \rightarrow X\,^1\Sigma^+)$ is in the mid ultraviolet, principally between 190 to 250 nm, and comes from a metastable state that is not easily seen in the laboratory. This emission in shuttle orbiter plumes is found to be dominated by two and three step chemistry of a minor amount of methane in the engine exhaust reacting with atmospheric atomic oxygen. Figure 2 shows the MSX satellite image of steady-state Cameron band radiance for the "High ram burn" reported in reference 3 compared to DSMC model calculations performed with the Transitional and Rarefied Axisymmetric Monte Carlo Plume (TRAMP) code. TRAMP is an axisymmetric DSMC code developed in parallel with the full-three dimensional SOCRATES code,[4] with the advantage that it converges approximately 10 times faster for axisymmetric cases. The dimension of the observed plume Cameron band radiance is roughly 30% larger than the DSMC model predictions for retrofire (into the ram) burns. Such a discrepancy is an indication that the mean-free-path of interacting species is not being treated correctly.
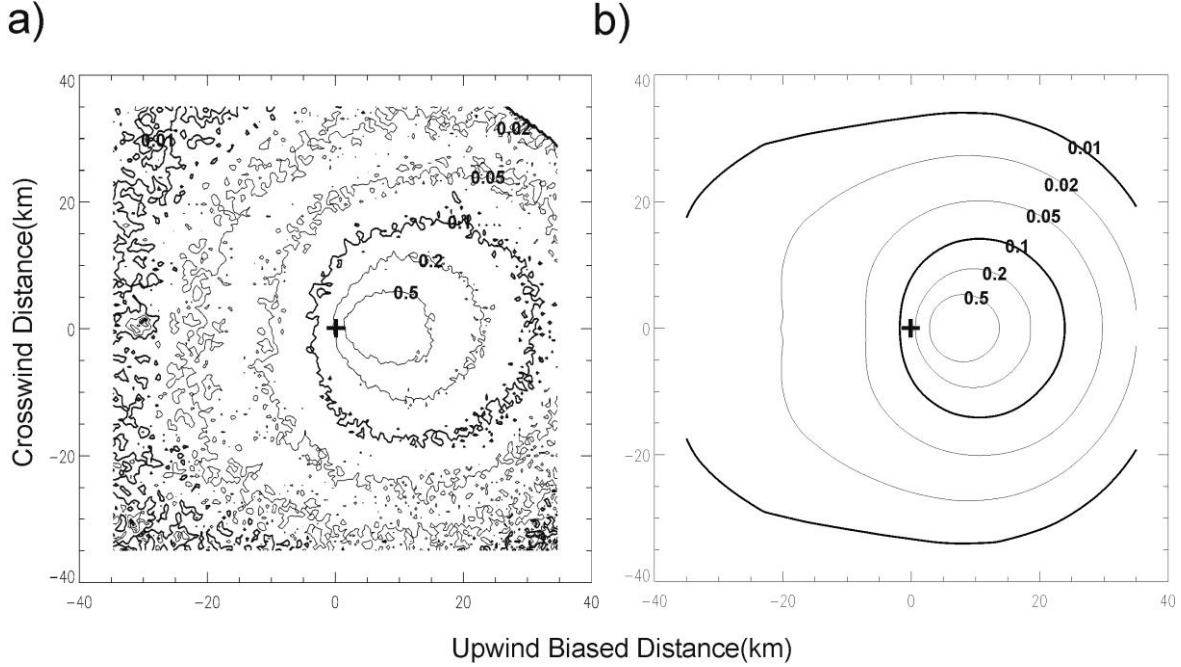
Figure 2. a) Cameron band radiance from a ram burn of shuttle orbiter engine at 298 km altitude. b) DSMC simulation of Cameron band radiance, showing smaller dimension for contour of a given fraction of the peak radiance. Contours are labeled in fractions of peak radiance. Atmospheric wind is entering from left at 46° to the view direction. The cross shows the location of the shuttle.

The mean free path is a function of the particle densities and the collision cross sections. Atmospheric densities are determined using the MSIS model,[5] which is described as having an uncertainty of ±15%. Consistent discrepancies greater than 15% for multiple plume observations were seen, so it is understood that the discrepancies are dominated by errors in the collision cross sections. The source of this discrepancy becomes apparent when the treatment of scattering cross sections by DSMC is examined.

The usual DSMC scattering treatment, which has been based on atomic and molecular interactions at thermal energies, deviates significantly from scattering that occurs at the hyperthermal collision energies (>1 eV) that are experienced at orbital velocities. The predicted hyperthermal energy collision repulsive interaction from the inverse-power law interaction potentials on which DSMC scattering has been based, varies significantly from the more exponential-like behavior that governs the actual interaction. The importance of including an exponential functionality to the size of particles at hyperthermal energies has been recognized earlier in DSMC treatment of sputtering.[6,7] Figure 2 shows the difference between the commonly used Lennard-Jones 6-12 and Born-Mayer exponential repulsive potentials fit at thermal and hyperthermal energies, respectively. While the Lennard-Jones functionality can fit the experimentally determined potential at thermal energies, but the r^{-12} repulsive contribution deviates strongly at hyperthermal energies. The Born-Mayer[8] exponential repulsive form,

$$V(r) = A \exp(-r/B);$$ (2)

where A and B are empirically determined range and softness parameters, respectively, doesn't produce a well, but can fit the measured potential over a broad range of hyperthermal energies. At hyperthermal collision energies the potential well will have little effect on a collision outcome. It is seen in Figure 3 that the Lennard-Jones potential fit to the He-He potential well produces much larger collision turning points at hyperthermal energies than the measured potential.
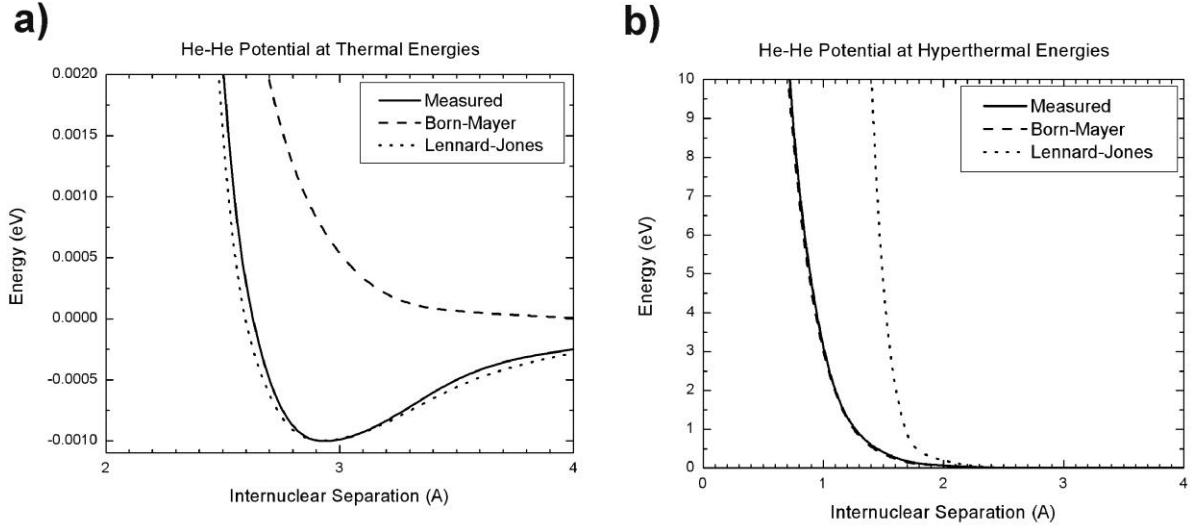
Figure 3. Lennard-Jones 6-12 and Born-Mayer exponential repulsive potential forms compared to measured He-He potential at a) thermal and b) hyperthermal energies.

In general, an inverse-power-law potential derived to match the energy dependence at some energy will consistently over predict representative hard sphere diameters by an increasing error as the collision energy increases.

The method chosen for defining variable hard sphere diameters derived from Born-Mayer potential functionality involves matching the velocity dependence at a reference energy (or a reference velocity or reference temperature, as mentioned earlier). The new diameters and cross sections are referred to here as Extended Variable Hard Sphere (EVHS) diameters and cross sections. EVHS diameters can also be used in combination with VSS scattering distributions, effectively defining an Extended Variable Soft Sphere (EVSS) applicable at hyperthermal energies. For valid EVHS and EVSS cross sections, however, it is important to use VHS cross section parameters from a reference energy that is high enough that the interaction is dominated by exponential repulsion and not influenced appreciably by long range attraction. A prescription for deriving EVHS model parameters from VHS functionality and incorporating EVHS cross sections into DSMC has been published earlier.[9] Typical cross section ratios derived from EVHS and VHS, matched at a relative collision velocity of 2.5 km/s are shown in Figure 4.
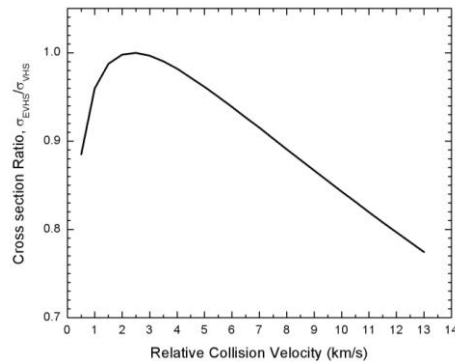

Figure 4. Velocity dependence of typical EVHS/VHS cross section ratio where the cross sections have been matched at a relative collision velocity of 2.5 km/s.

This paper includes derivation of viscosity and collision frequency formulas based on EVHS Born-Mayer potential functionality and verification through comparison of viscosity and shock density profiles for VHS and EVHS models. Validation at hyperthermal energies is performed through applying EVHS to modeling the Cameron band emission data shown in Figure 2a.

2. VISCOSITY AND COLLISION FREQUENCY OF EVHS MODEL

For the numerical results obtained with the EVHS model to agree with experimental data one needs to match viscosity of simulated gas with that of the real one. To this end, let us derive the temperature dependent expression for the viscosity of an EVHS gas. The 1st order approximation to the coefficient of viscosity in a single species gas may be written[10] as

$$\mu = \frac{5/8\sqrt{\pi m k T}}{\left(\frac{m}{4kT}\right)^4 \int_0^\infty g^7 \sigma_\mu(g) e^{-\frac{mg}{4kT}} dg}, \qquad (3)$$

where m is molecular mass, T is gas temperature, g is the relative collision velocity, and σ_μ is the viscosity cross section. For EVHS, similar to VHS, one can write

$$\sigma_\mu = \frac{2}{3}\pi d^2,$$

where d is the collision diameter that for EVHS generally depends on the relative translational energy E_{tr}, since

$$E_{tr} \equiv \frac{m_r g^2}{2} = A e^{\frac{-d}{B}}, \text{ and therefore}$$

$$\sigma_\mu = \frac{2}{3}\pi B^2 \log^2\left(\frac{mg^2}{4A}\right). \qquad (4)$$

Here, A and B are the parameters of the EVHS potential. Substituting Eq (4) into Eq (3), and conducting change of variables $g = x\sqrt{\frac{4kT}{m}}$, we obtain

$$\mu = \frac{5/8\sqrt{\pi m k T}}{\frac{2}{3}\pi B^2 \int_0^\infty x^7 e^{-x^2} \log^2(Cx) dx}, \qquad (5)$$

where $C = \frac{kT}{A}$. The integration of this expression results in an analytic form for the viscosity coefficient,

$$\mu = \frac{15\sqrt{\pi m k T}}{16\pi B^2}\left\{3\log C + 11\log C - 6\gamma\gamma\log C + 6 + \frac{\pi^2}{2} - 11\gamma + 3\gamma^2\right\}, \qquad (6)$$

where $\gamma = 0.5772157$. Similarly, the expression for the collision frequency of EVHS molecules may be obtained as

$$v = n\langle\sigma_t g\rangle = n\sqrt{\frac{2}{\pi}}\left(\frac{m_r}{kT}\right)^{3/2}\int_0^\infty \sigma_t(g)g^3 e^{\frac{-m_r g^2}{2kT}} dg = 4\sqrt{\pi}B^2\left(\frac{2kT}{m_r}\right)^{1/2}\left\{\frac{1}{2}\log^2 C + (1-\gamma)\log C + \frac{1}{12}\pi^2 - \gamma + 0.5\gamma^2\right\}.$$

3. NORMAL SHOCK WAVE

The first application of the EVHS potential presented in this paper is the structure of a normal shock wave. The availability of experimental data[11] on shock wave profiles in argon, as well as the measured viscosity data[12] for argon in a wide range of temperatures, allows model validation to be performed. In addition to the EVHS model, the standard VHS model has also been used. Prior to the DSMC runs, the viscosity data were analyzed, and EVHS and VHS parameters were chosen so that the DSMC viscosity agrees reasonably with the measured values. The EVHS parameters used are $A = 1.023 \times 10^{-14}$J, $B = 0.253$ Å at a reference temperature of 273K. For the VHS model, $d_{ref} = 3.73$ Å and $\omega = 0.67$. As was shown in reference **9**, the parameters of the EVHS model A and B may be related to the

VHS parameters d_{ref} and ω, if one assumes $(E_{tr})_{\text{EVHS}}=(E_{tr})_{\text{EVHS}}$ and $(E_{tr})'_{\text{EVHS}}=(E_{tr})'_{\text{EVHS}}$ at some reference temperature. In this case, $A = e^{\frac{2}{\omega-0.5}} kT_{ref}\left(\Gamma(2.5-\omega)\right)^{-0.5}$, $B = \dfrac{\omega-0.5}{2}d_{ref}$.

The above EVHS and VHS parameters were selected to provide a good approximation for the viscosity of the EVHS and VHS models as compared to the measured profiles, shown in Fig. 5. Note that there is some difference at lower temperatures (below about 500 K), with the models producing somewhat higher viscosity than that observed in the experiment, but the difference becomes negligible at higher temperatures. It is recommended that, where possible, EVHS parameters be selected by direct fitting to viscosity in the highest available temperature range. In some cases, however, it may be that some assumed VHS parameters are available even though the fundamental transport properties are not. In fact, this is the case for the SOCRATES example shown below. In this case, the relations above provide the means to obtain EVHS parameters from given VHS parameters. We note strongly that the two sets of cross sections will cross at the specified value of E_{ref} (sometimes specified as T_{ref}) and diverge at higher energies, so the conversion should be done at the highest possible value of E_{ref}. A low reference value, such as $T_{ref} = 273$K, will match the cross sections in a thermal regime which may be substantially influenced by attractive forces and will reduce the validity of the EVHS assumptions. For example, the VHS parameters recommended for Ar in reference **10**: $T_{ref} = 273$K, $d_{ref} = 4.17$, and $\omega = 0.81$, begin to deviate from the measured viscosity in the range T>600K. If the VHS parameters recommended above for the $M = 3.8$ shock are converted to their high-temperature equivalent $d_{ref} = 3.09$ and $\omega = 0.67$ at $T_{ref} = 2500$ K, then the successive EVHS conversion of the latter would predict $A = 6.67e$-15 J, $B = 0.263A$. These produce similarly good agreement with known viscosity in the 600-3000K range as the A and B values obtained from direct fitting of the viscosity.
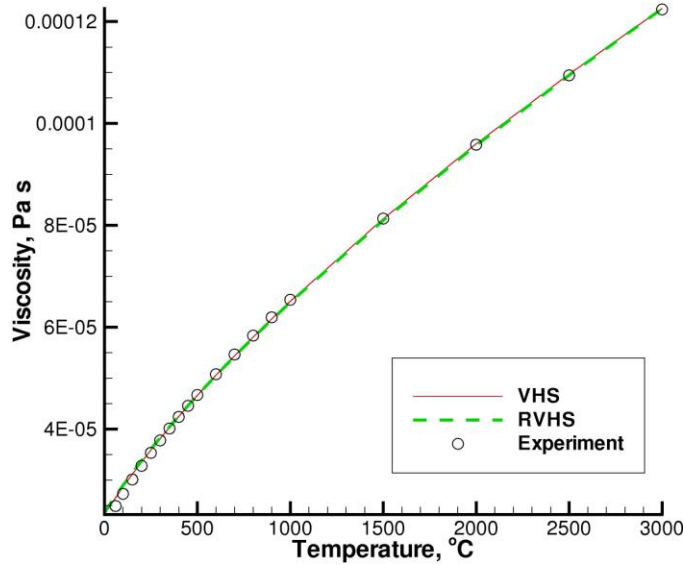

Figure 5. Comparison of DSMC and measured viscosity in argon.

Comparison of the computed and measured normalized density profiles for $M = 3.8$ is given in Fig. 6. In this plot, similar to those in reference **11**, the distance variable is normalized by the mean free path in front of the shock wave, $\lambda = 1.098$mm for $T = 300$ K and $p = 50$ mTorr; the gas density is normalized as $\dfrac{\rho - \rho_{-\infty}}{\rho_{\infty} - \rho_{-\infty}}$. It is clearly seen that the computed density values are very close to the measured one. There is a small difference in the shallow part of the shock wave, with the computed profiles appearing to be more viscous, which is attributed to higher DSMC viscosity at lower temperatures (see Fig. 5).
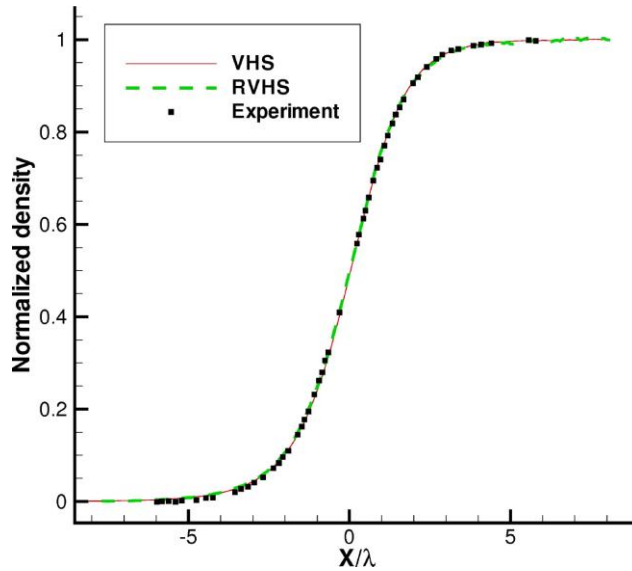
Figure 6. Computed and measured density profiles inside a shock wave.

4. VALIDATION AT HYPERTHERMAL ENERGIES

The data used for validation of EVHS at hyperthermal energies is the "High ram bun" shown in Figure 2a. The High ram burn was a 37 second retrofire burn of a single 6000 lbf thrust space shuttle Orbital Maneuvering System engine at an altitude of 298 km in the earth's umbra. Atmospheric conditions determined by MSIS were: a total number density of 2.78 x 10^8 cm^{-3}, a temperature of 717 K and a mole fraction composition of $O/N_2/O_2$::0.904/0.093/0.003. More characterizing parameters are given in greater detail in reference **3**.

In the original analysis Cameron band radiance was determined through agreement with DSMC modeling to result from two and three step chemistry from a minor amount (1% mole fraction) of methane in the plume:

$$CH_4 + O \rightarrow CH_3 + OH \tag{R1}$$
$$CH_3 + O \rightarrow CO(a) + H_2 + H \tag{R2}$$
$$CH_3 + O \rightarrow CH_2 + OH \tag{R3}$$
$$CH_2 + O \rightarrow CO(a) + H_2 \tag{R4}$$
$$CO(a) \rightarrow CO + h\nu \tag{R5}$$

Reactions (R2) and (R4) are previously unknown chemistry which were assigned activation energies of 100 and 50 kcal/mole, respectively, to obtain agreement with plume shapes. Spectator stripping product scattering distributions were uses for Reactions (R1) and (R3). That distribution for Reaction (R1) was found to be important in reproducing the observed plume shape, and subsequently has been verified in hyperthermal molecular beam laboratory experiments.[13] The remaining discrepancies in plume size and shape predicted by plume modeling, shown in Figure 2, were the inspiration for postulating the importance of the EVHS treatment. The axisymmetric DSMC TRAMP code was modified to use EVHS cross sections. VHS reference cross sections at reference velocities ranging from 2 to 8 km/s were used to generate EVHS characterizing parameters. Figure 7 shows the comparison of the data with the EVHS computed plume, with all the remaining input parameters remaining the same, showing a significant improvement in agreement in the size of the contours.
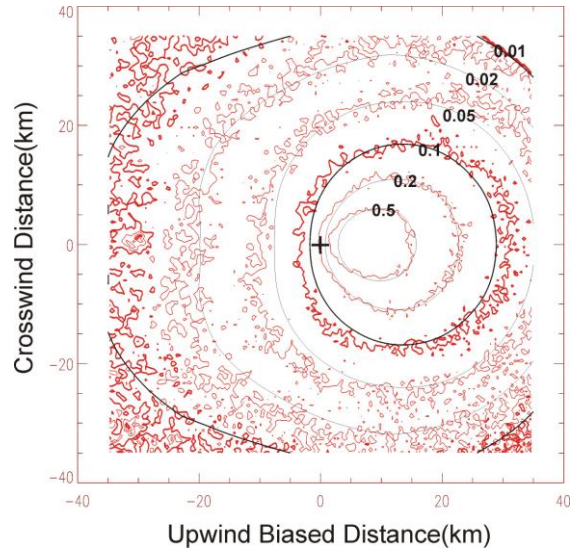
Figure 7. Comparison of observed Cameron Band radiance with EVHS modeled radiance.

The TRAMP code uses a global value of the viscosity coefficient ω. The value that had been used predominantly in past studies, including the cases shown in Figures 2b and 7, was $\omega = 0.75$. Before including the EVHS model into TRAMP an attempt to increase the mean free path for molecules traveling at hyperthermal velocities was done by increasing ω to 0.9 without changing the species reference diameters and energies. That change indeed increased the size of the radiance contours but also, interestingly, modified the shape of the 0.5 (of peak radiance) contour to more closely match its "egg" shape in the data. It was anticipated that the EVHS addition might accomplish the same improvement in shape. The comparison in Figure 7 shows a small improvement in shape but indicates that there are still discrepancies that indicate a larger ω may relevant to the collisions governing the shape of the radiance. The ω = 0.75 value was determined from examining viscosity coefficients for stable gases, all of which have closed electronic structures. Radicals, such as atomic oxygen have unpaired electrons which would be expected to produce softer repulsive potentials in collisions with closed shell structures. Considering that the spatial distribution at the level of the 0.5 contour is probably most strongly influenced by O + CH_4 collisions $\omega = 0.8$ was use for an EVHS analysis. The result, shown in Figure 8, shows an improved match in shapes of the 0.5 contour and generally improved agreement among all the contours.
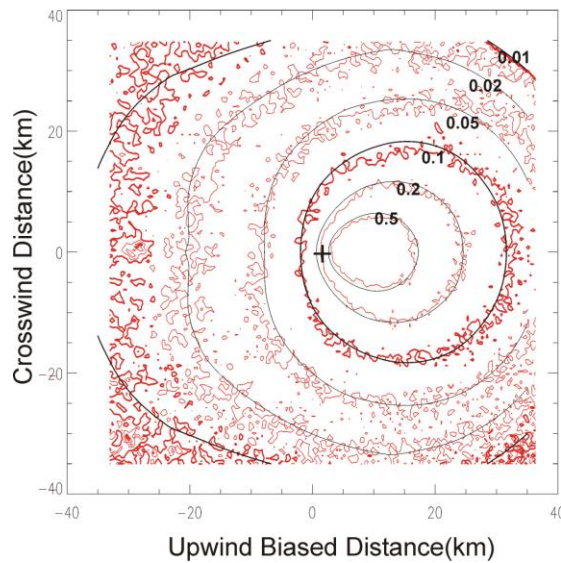

Figure 6. Comparison of observed Cameron Band radiance with EVHS modeled radiance with $\omega = 0.8$. Data have been offset ~2 km to the right, consistent with the shuttle beacon tracking uncertainty.

5. CONCLUSIONS

A simple modification of the VHS collision model is described that will be useful for DSMC cases where the typical collision energy greatly exceeds the collision energies typical of thermal viscosity measurements. For flowfields with hyperthermal collision energies, the EVHS and EVSS can be expected to provide a superior method of extrapolation from known thermally-based VHS parameters. Care must be taken in applying this model, since it assumes that the VHS parameters used as a starting point reflect a regime dominated by a repulsive potential. If the VHS parameters are based on viscosity values that reflect a significant contribution from attractive forces, then the validity of this method of predicting the high-energy collision cross section is lost.

We have verified the ability of this model to continue to reproduce the given viscosity data near the reference temperature. Validation data for very high temperature or very high energy flows are rare, but we have provided one comparison case with measurements that validate the ability of this model to improve the physical realism of the collisions predicted by DSMC. One day, it may be that any viscosity-based simplified collision model will be unnecessary as computational chemistry tools may provide reasonable values for elastic collision cross sections (as well as inelastic cross sections) over the full range of energies. First examples of this capability have been demonstrated by Tokumasu and by Ozawa **[refs].**

7. REFERENCES

[1] Bird, G. A., "Monte Carlo simulation in and engineering context," *Progr. Astro. Aero*. Vol. 74, pp. 239-255 (1981).

[2] Koura, K. and Matsumoto, H, "Variable soft sphere molecular model for inverse-power-law or Lennard-Jones potential," *Phys. Fluids A*, Vol. 3, pp/. 2459-2465 (1991).

[3] Dimpfl, W. L., Light, G. C., and Bernstein, L. S., "Molecular Dynamics from Remote Observations of CO(a) from Space Shuttle Plumes," *J. Spacecraft & Rockets*, Vol. 42, No. 2, pp. 352-362 (2005).

[4] Elgin, J. B., Cooke, D. C., Tautz, M. F., and Murad, E., "Modeling of Atmospherically Induced Gas Phase Optical Contamination from Orbiting Spacecraft," *Journal of Geophysical Research*, Vol. 95, No. A8, pp. 12197-12208 (1990).

[5] Hedin, A. E., "MSIS-86 Thermospheric Model," *J. Geophys. Res.*, Vol. 92, No. A5, 1987, pp. 4649-4662.

[6] Kersch, A., Morokoff, W., and Werner, Chr., "Self consistent simulation of sputter deposition with the Monte Carlo method," *J. Appl. Phys*. Vol 75 (4), pp.2278-2285 (1994).

[7] Kobayashi, T., "Computer simulation of gas rarefaction effects and film deposition charactristics in a magnetron sputtering apparatus," *Applied Surface Science*, Vol. 169-170, pp. 405-409 (2001).

[8] Born, M. and Mayer, J. E., "Zur Gittertheorie der Ionenkristalle," *Z. Physik*, Vol. 75, p. 1 (1932).

[9] Dimpfl, W. L. and "Bernstein, L. S., "Improvements in Modeling Radiant Emission from the Interaction Between Spacecraft Emanations and the Residual Atmosphere in LEO," *Proceedings of the AMOS Technical Conference*, (2005).

[10] S. Chapman and T.G. Cowling, "The Mathematical Theory of Non-Uniform Gases," Cambridge University Press, Cambridge (1970).

[11] S. Alsmeyer, "Density profiles in argon and nitrogen shock waves measured by the absorption of an electron beam," *J. Fluid Mech*. 74, 497 (1976).

[12] J. Kestin, K. Knierim, E. A. Mason, B. Najafi, S. T. Ro, and M. Waldman, "Equilibrium and transport properties of the noble gases and their mixtures at low density," *J. Phys. Chem. Ref. Data* **13**, 229 (1984).

[13] Garton, D, "Hyperthemal Reactions of O(^{3}P) with Hydrogen and Methane," Montana State University Ph. D. Thesis, April 2004.